

# Central $\mu^+\mu^-$ production via photon-photon fusion in proton-proton collisions with proton dissociation

**Gustavo G. da Silveira<sup>a,b</sup> Laurent Forthomme<sup>a</sup> Krzysztof Piotrzkowski<sup>a</sup> Wolfgang Schäfer<sup>c</sup> and Antoni Szczurek<sup>c,d</sup>**

<sup>a</sup>*Centre for Cosmology, Particle Physics and Phenomenology (CP3), Université Catholique de Louvain, B-1348 Louvain-la-Neuve, Belgium*

<sup>b</sup>*High and Medium Energy Group, Instituto de Física e Matemática, Universidade Federal de Pelotas, Caixa Postal 354, CEP 96010-900, Pelotas, RS, Brazil*

<sup>c</sup>*Institute of Nuclear Physics PAN, PL-31-342 Kraków, Poland*

<sup>d</sup>*University of Rzeszów, PL-35-959 Rzeszów, Poland*

*E-mail:* [gustavo.silveira@cern.ch](mailto:gustavo.silveira@cern.ch), [laurent.forthomme@uclouvain.be](mailto:laurent.forthomme@uclouvain.be),  
[krzysztof.piotrzkowski@uclouvain.be](mailto:krzysztof.piotrzkowski@uclouvain.be), [wolfgang.schafer@ifj.edu.pl](mailto:wolfgang.schafer@ifj.edu.pl),  
[antoni.szczurek@ifj.edu.pl](mailto:antoni.szczurek@ifj.edu.pl)

**ABSTRACT:** We present a formalism which uses fluxes of equivalent photons including transverse momenta of the intermediate photons. The formalism reminds the familiar  $k_t$ -factorization approach used, e.g., to study the two-photon production of  $c\bar{c}$  or  $b\bar{b}$  pairs. The results of the new method are compared with those obtained using the code LPAIR, and a good agreement is obtained. The inclusion of the photon transverse momenta is necessary in studies of correlation observables. We present distributions for the dimuon invariant mass, transverse momentum of the muon pair and relative azimuthal angle between muons separately for elastic-elastic, elastic-inelastic, inelastic-elastic and inelastic-inelastic mechanisms. For typical experimental cuts all mechanisms give similar contributions. The results are shown for different sets of cuts relevant for the LHC experiments. The cross sections in different regions of phase space depend on  $F_2$  structure function in different regions of  $x$  and  $Q^2$ . A comment on  $F_2$  is made.

**KEYWORDS:** two-photon reaction,  $k_t$ -factorization, Monte Carlo event generator, muon pair production, equivalent photon approximation

---

## Contents

<b>1</b>	<b>Introduction</b>	<b>1</b>
<b>2</b>	<b>Lepton pair production including electromagnetic dissociation of protons at high energies: a <math>k_T</math>-factorization approach</b>	<b>3</b>
2.1	Kinematics	3
2.2	Pair production amplitude	4
2.3	Off-shell cross section	5
2.3.1	$\gamma^*\gamma^* \rightarrow \ell^+\ell^-$	5
2.4	Decorrelation of leptons	7
<b>3</b>	<b>Results of <math>k_T</math>-factorization approach</b>	<b>7</b>
<b>4</b>	<b>LPAIR Monte Carlo studies</b>	<b>12</b>
4.1	LPAIR event generator	12
4.2	Some LPAIR results with detector acceptance	14
<b>5</b>	<b>LPAIR vs. <math>k_T</math>-factorization approach</b>	<b>16</b>
<b>6</b>	<b>Conclusions</b>	<b>18</b>

---

## 1 Introduction

The production of lepton pairs via  $\gamma\gamma$ -fusion in hadron-hadron collisions has been studied for a long time. Substantial interest in the exclusive lepton pair production was generated by the work [1], where it was proposed to use this process, which is calculable in QED, to measure the luminosity of a collider. However, regarding the investigation proposed in this paper, we are interested in the multiperipheral collisions, which are presented in Figure 1: elastic interaction with both protons intact in the final state (Figure 1a), one proton dissociates into a hadronic system in the final state (Figure 1b), and both protons dissociate (Figure 1c).

Such calculations are typically performed in the equivalent photon approximation [2]. Here the ingredients are the photon fluxes, which are fully specified by the electromagnetic form factors of the colliding hadrons, and off-shell cross sections (or density matrices) that describe the  $\gamma^*(q_1^2)\gamma^*(q_2^2) \rightarrow \ell^+\ell^-$  process. It is also straightforward to include the breakup of the incoming protons: here the relevant fluxes will be calculable in terms of the total (virtual) photoabsorption cross sections – or structure functions – of the beam particles. All the relevant expressions for the photon fluxes are given in the review [2], and also certain off-shell cross sections can be found there.

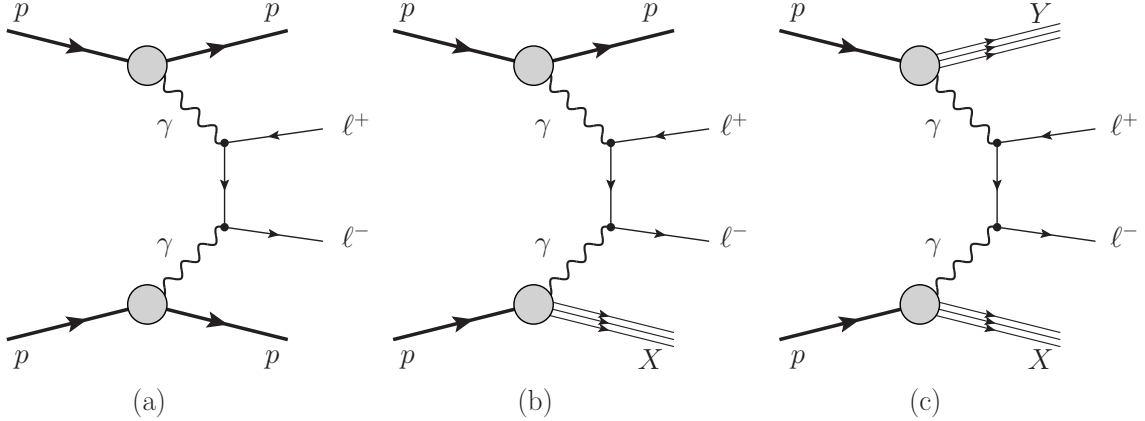


**Figure 1.** Diagrams representing the multiperipheral two-photon processes studied in this paper: (a) elastic process, (b) single-dissociative and (c) double-dissociative process. In all three cases it is possible to study lepton pair production, like  $e^+e^-$ ,  $\mu^+\mu^-$  and  $\tau^+\tau^-$ , whereas  $X$  and  $Y$  represent the hadronic systems resulting from the proton dissociation.

As will be discussed in the present paper, the calculation of inelastic unintegrated photon fluxes requires knowledge of the proton structure functions in a broad range of  $x$  (quark/antiquark longitudinal momentum fraction with respect to the proton) and  $Q^2$  (photon virtuality). In the deep-inelastic regime, the structure functions (parton distributions) are related to the proton's partonic structure and undergo DGLAP evolution equations. At low virtualities the structure function cannot be calculated easily from first principles and has to be rather measured. There are some simple models to extend the partonic  $F_2$  to nonperturbative model (e.g., see Ref. [3]). This model nicely describes virtuality dependence of the Gottfried Sum Rule [4]. The very low  $Q^2$  region was parametrized in Ref. [5] including pronounced resonance states by fitting data from SLAC and JLAB.

In this work we also bring attention to the fact that the relevant formalism for  $\gamma\gamma$ -fusion reactions in the high-energy limit can be understood as a type of  $k_T$ -factorization, where the photon fluxes play the role of "unintegrated" (transverse momentum-dependent) photon densities. Indeed, as will be seen below, the cross section takes the exactly analogous form as the  $k_T$ -factorization formula for  $q\bar{q}$  jet production via gluon-gluon fusion (e.g., see Ref. [6].)

Here we go beyond what is available in the literature by addressing distributions in the transverse momentum of the muon pair as well as the azimuthal decorrelation of muons. We also use a variety of modern parametrizations of the proton structure functions and discuss the uncertainties related to them.

Another quantitative description of lepton pair production is the LPAIR event generator [7], which is based on the calculation for two-photon processes [8], and also has the possibility to include proton dissociative processes. We compare the results of our  $k_T$ -factorization approach to the results obtained with LPAIR.

Considering the two-photon production of low- and high-mass systems, this work is also motivated by the fact that the experimental results for exclusive dimuon production with the CMS detector indicate that the description provided by LPAIR is not accurate for

large transverse momentum of the dimuons [17, 19]. Then, in this paper we explore the corresponding phase space using the LPAIR and the theoretical  $k_T$ -factorization approach, in order to understand the possible effects that can contribute for this discrepancy between data and theory, which can be related to the proton structure functions or rescattering corrections not taken into account in the event generator.

This paper is organized as follows: in Section 2 we describe the theoretical approach. Next, the results obtained with the proposed approach are presented in Section 3. In Sec. 4 we study the exclusive  $\mu^+\mu^-$  production with the use of LPAIR Monte Carlo generator. Then, Section 5 presents a dedicated survey oriented to compare the theoretical predictions. Finally, our conclusions are summarized in Section 6.

## 2 Lepton pair production including electromagnetic dissociation of protons at high energies: a $k_T$ -factorization approach

### 2.1 Kinematics

We want to describe ultrarelativistic collisions involving particles  $A, B$  with four-momenta  $p_A, p_B$  which fulfill the on-shell conditions  $p_A^2 = m_A^2, p_B^2 = m_B^2$ . It is useful to introduce the light-like momenta:

$$p_1 = p_A - \frac{m_A^2}{\tilde{s}} p_B, \quad p_2 = p_B - \frac{m_B^2}{\tilde{s}} p_A, \quad (2.1)$$

where

$$\tilde{s} = s \cdot \frac{1}{2} \left\{ 1 + \sqrt{1 - \frac{4m_A^2 m_B^2}{s^2}} \right\}, \quad s \equiv 2(p_A \cdot p_B), \quad (2.2)$$

so that  $p_1^2 = p_2^2 = 0$ . For an arbitrary four-vector  $a$ , we then introduce the Sudakov-decomposition:

$$a = \alpha p_1 + \beta p_2 + a_\perp. \quad (2.3)$$

Correspondingly, we have the Gribov-decomposition of the metric tensor:

$$g_{\mu\nu} = g_{\mu\nu}^\perp + \frac{p_{1\mu} p_{2\nu} + p_{2\mu} p_{1\nu}}{(p_1 \cdot p_2)}. \quad (2.4)$$

The euclidean components of the transverse part of a four vector  $a_\mu^\perp \equiv g_{\mu\nu}^\perp a_\nu$  will be denoted by  $\vec{a}_T$ , so that:

$$(a^\perp \cdot b^\perp) = -\vec{a}_T \cdot \vec{b}_T. \quad (2.5)$$

In the high energy limit adopted by us, we regard as small all quantities of the type:

$$\epsilon \sim \frac{m^2}{s}, \frac{\vec{p}_T^2}{s}, \frac{m|\vec{p}_T|}{s}, \quad (2.6)$$

where  $m, \vec{p}_T$  stand for the mass and transverse momentum of any of the participating particles. In particular, we have that:

$$s = E_{\text{cm}}^2 (1 + \mathcal{O}(\epsilon)), \quad 2(p_1 \cdot p_2) = s (1 + \mathcal{O}(\epsilon)). \quad (2.7)$$

Our calculations will be accurate to power accuracy in the small parameter  $\epsilon$ , and below that we will no longer distinguish between quantities differing by  $\mathcal{O}(\epsilon)$  amounts wherever possible.

## 2.2 Pair production amplitude

Our discussion of the pair production amplitude follows, with small notational changes, closely the discussion in [9]. Let the four-momenta of leptons be  $p_+$  and  $p_-$ , then, in the Feynman gauge, the amplitude takes the form:

$$M = -i \frac{(4\pi\alpha_{\text{em}})^2}{q_1^2 q_2^2} V_\mu^{A \rightarrow X}(p_A, p_X) g_{\mu\alpha} \bar{u}_\lambda(p_-) T_{\alpha\beta} v_{\bar{\lambda}}(p_+) g_{\beta\nu} V_\nu^{B \rightarrow Y}(p_B, p_Y), \quad (2.8)$$

with

$$T_{\alpha\beta} = \gamma_\alpha \frac{\hat{q}_1 - \hat{p}_+ + m}{(q_1 - p_+)^2 - m^2} \gamma_\beta + \gamma_\beta \frac{\hat{q}_2 - \hat{p}_+ + m}{(q_2 - p_+)^2 - m^2} \gamma_\alpha, \quad \hat{q}_1 \equiv q_{1\mu} \gamma_\mu \text{ etc.} \quad (2.9)$$

The vertex describing the transitions  $A \rightarrow X$  is:

$$\sqrt{4\pi\alpha_{\text{em}}} V_\mu^{A \rightarrow X}(p_A, p_X) = \langle X(p_X) | j_\mu^{\text{em}}(0) | A(p_A) \rangle, \quad (2.10)$$

and its square is related to the hadronic tensor:

$$W_{\mu\nu}^A(q) \equiv \sum_X (2\pi)^3 \delta^{(4)}(p_X - p_A - q) V_\mu^{\dagger A \rightarrow X}(p_A, p_X) V_\nu^{A \rightarrow X}(p_A, p_X). \quad (2.11)$$

Using the Gribov decomposition of the metric tensor, one can show that the leading contribution in the high energy limit is obtained by substituting in the photon propagators:

$$g_{\mu\alpha} \rightarrow \frac{2}{s} p_{2\mu} p_{1\alpha}, \quad g_{\beta\nu} \rightarrow \frac{2}{s} p_{2\nu} p_{1\beta}. \quad (2.12)$$

After this substitution, we obtain for the production amplitude the compact ‘‘impact factor’’ [10, 11] representation:

$$\mathcal{M} = -is \frac{(8\pi\alpha_{\text{em}})^2}{q_1^2 q_2^2} N_1(q_1) B_{\lambda\bar{\lambda}}(k_+, k_-; q_1, q_2) N_2(q_2), \quad (2.13)$$

where

$$\begin{aligned} N_1(q_1) &= \frac{1}{s} p_{2\mu} V_\mu^{A \rightarrow X}(p_A, p_X), \quad N_2(q_2) = \frac{1}{s} p_{1\nu} V_\nu^{B \rightarrow Y}(p_B, p_Y), \\ B_{\lambda\bar{\lambda}}(k_+, k_-; q_1, q_2) &= \frac{1}{s} p_{1\alpha} p_{2\beta} \bar{u}_\lambda(k_-) T_{\alpha\beta} v_{\bar{\lambda}}(k_+). \end{aligned} \quad (2.14)$$

The normalization is the standard one:

$$d\sigma(AB \rightarrow X \ell^+ \ell^- Y) = \frac{1}{2s} |\overline{\mathcal{M}}|^2 d\Phi(s; \{p_i\}_{i \in X}, \{p_j\}_{j \in Y}, k_+, k_-), \quad (2.15)$$

The photon  $q_1, q_2$  four-vectors have the Sudakov decomposition:

$$q_i = \alpha_i p_1 + \beta_i p_2 + q_{i\perp}, \quad q_i^2 = \alpha_i \beta_i s - \vec{q}_{T_i}^2, \quad (2.16)$$

where from the on shell conditions of  $p_A^2 = m_A^2, p_X^2 = M_X^2, p_B^2 = m_B^2, p_Y^2 = M_Y^2$ , we obtain the small Sudakov parameters

$$\beta_1 = -\frac{M_X^2 - m_A^2 + \vec{q}_{T_1}^2 + \alpha_1 m_A^2}{(1 - \alpha_1)s}, \quad \alpha_2 = -\frac{M_Y^2 - m_B^2 + \vec{q}_{T_2}^2 + \beta_2 m_B^2}{(1 - \beta_2)s}, \quad (2.17)$$

as well as the virtualities of photons

$$\begin{aligned} Q_1^2 \equiv -q_1^2 &= \frac{1}{1-\alpha_1} \left[ \vec{q}_{T1}^2 + \alpha_1(M_X^2 - m_A^2) + \alpha_1^2 m_A^2 \right], \\ Q_2^2 \equiv -q_2^2 &= \frac{1}{1-\beta_2} \left[ \vec{q}_{T2}^2 + \beta_2(M_Y^2 - m_B^2) + \beta_2^2 m_B^2 \right]. \end{aligned} \quad (2.18)$$

The cross section differential in the lepton rapidities and transverse momenta can be written in the form familiar from the  $k_T$ -factorization:

$$\frac{d\sigma(AB \rightarrow X\ell^+\ell^-Y)}{dy_+ dy_- d^2\vec{p}_{T+} d^2\vec{p}_{T-}} = \int \frac{d^2\vec{q}_{T1}}{\pi\vec{q}_{T1}^2} \frac{d^2\vec{q}_{T2}}{\pi\vec{q}_{T2}^2} \mathcal{F}_{\gamma^*/A}^{(i)}(x_1, \vec{q}_{T1}) \mathcal{F}_{\gamma^*/B}^{(j)}(x_2, \vec{q}_{T2}) \frac{d\sigma^*(p_+, p_-; \vec{q}_{T1}, \vec{q}_{T2})}{dy_+ dy_- d^2\vec{p}_{T+} d^2\vec{p}_{T-}}, \quad (2.19)$$

where

$$x_1 = \frac{m_{\perp+}}{\sqrt{s}} e^{y_+} + \frac{m_{\perp-}}{\sqrt{s}} e^{y_-}, \quad x_2 = \frac{m_{\perp+}}{\sqrt{s}} e^{-y_+} + \frac{m_{\perp-}}{\sqrt{s}} e^{-y_-}, \quad m_{\perp\pm} = \sqrt{\vec{p}_{T\pm}^2 + m_\ell^2}.$$

The unintegrated photon densities  $\mathcal{F}_{\gamma^*/A}^{(i)}(x, \vec{q}_{T2})$ , where  $(i = \text{el}, \text{inel})$  read explicitly:

$$\mathcal{F}_{\gamma/A}^{(\text{el})}(\alpha, \vec{q}_T^2) = \frac{\alpha_{\text{em}}}{\pi} (1-\alpha) \left[ \frac{\vec{q}_T^2}{\vec{q}_T^2 + \alpha^2 m_A^2} \right]^2 \frac{4m_p^2 G_E^2(Q^2) + Q^2 G_M^2(Q^2)}{4m_p^2 + Q^2} \left( 1 - \frac{Q^2 - \vec{q}_T^2}{Q^2} \right), \quad (2.20)$$

$$\begin{aligned} \mathcal{F}_{\gamma/A}^{(\text{inel})}(\alpha, \vec{q}_T^2) &= \frac{\alpha_{\text{em}}}{\pi} (1-\alpha) \int_{M_{\text{thr}}^2}^{\infty} \frac{dM_X^2 F_2(M_X^2, Q^2)}{M_X^2 + Q^2 - m_p^2} \left( 1 - \frac{Q^2 - \vec{q}_T^2}{Q^2} \right) \\ &\quad \times \left[ \frac{\vec{q}_T^2}{\vec{q}_T^2 + \alpha(M_X^2 - m_A^2) + \alpha^2 m_A^2} \right]^2. \end{aligned} \quad (2.21)$$

Notice that it is a property of the high-energy limit that fluxes of transverse and longitudinal virtual photons are equal and only the structure function  $F_2 = 2xF_1 + F_L$  appears.

## 2.3 Off-shell cross section

### 2.3.1 $\gamma^* \gamma^* \rightarrow \ell^+ \ell^-$

The second ingredient of our calculation is the off-shell cross section for the fusion of virtual photons, which reads<sup>1</sup>:

$$\frac{d\sigma^*(p_+, p_-; \vec{q}_{T1}, \vec{q}_{T2})}{dy_1 dy_2 d^2\vec{p}_{T+} d^2\vec{p}_{T-}} = \frac{\alpha_{\text{em}}^2}{\vec{q}_{T1}^2 \vec{q}_{T2}^2} \sum_{\lambda, \bar{\lambda}} \left| B_{\lambda\bar{\lambda}}(p_+, p_-; q_1, q_2) \right|^2 \delta^{(2)}(\vec{q}_{T1} + \vec{q}_{T2} - \vec{p}_{T+} - \vec{p}_{T-}).$$

We parametrize the lepton four-momenta in terms of their Sudakov-parameters as:

$$p_{\pm} = \alpha_{\pm} p_1 + \beta_{\pm} p_2 + p_{\pm\perp}, \quad \beta_{\pm} = \frac{\vec{p}_{T\pm}^2 + m^2}{\alpha_{\pm} s}. \quad (2.22)$$

<sup>1</sup>Note that (the transverse) virtual photons carry the linear polarizations parallel to  $\vec{q}_{T1}, \vec{q}_{T2}$ , and the averaging over photon polarizations is in fact effected by the azimuthal integrations in Eq.(2.2).

Then, for the off-shell cross section, a particularly simple form can be obtained in terms of the variables [9]:

$$z_{\pm} = \frac{\alpha_{\pm}}{\alpha}, \quad \vec{k}_T = z_- \vec{p}_{T+} - z_+ \vec{p}_{T-}. \quad (2.23)$$

The familiar structures

$$\begin{aligned} \Phi_0 &= \frac{1}{(\vec{k}_T + z_+ \vec{q}_{T2})^2 + \varepsilon^2} - \frac{1}{(\vec{k}_T - z_- \vec{q}_{T2})^2 + \varepsilon^2}, \\ \vec{\Phi}_T &= \frac{\vec{k}_T + z_+ \vec{q}_{T2}}{(\vec{k}_T + z_+ \vec{q}_{T2})^2 + \varepsilon^2} - \frac{\vec{k}_T - z_- \vec{q}_{T2}}{(\vec{k}_T - z_- \vec{q}_{T2})^2 + \varepsilon^2}, \end{aligned} \quad (2.24)$$

with  $\varepsilon^2 = m_\ell^2 + z_+ z_- + Q_1^2$ , enter the off-shell matrix element (see e.g. [9]<sup>2</sup>):

$$\begin{aligned} \sum_{\lambda, \bar{\lambda}} \left| B_{\lambda \bar{\lambda}}(p_+, p_-; q_1, q_2) \right|^2 &= \frac{1}{s^2} \sum_{\lambda, \bar{\lambda}} \left| p_{1\alpha} p_{2\beta} \bar{u}_\lambda(p_-) T_{\alpha\beta} v_{\bar{\lambda}}(p_+) \right|^2 \\ &= 2z_+ z_- \vec{q}_{T1}^2 \left[ \underbrace{4z_+^2 z_-^2 \vec{q}_{T1}^2 \Phi_0^2}_L \right. \\ &\quad + \underbrace{(z_+^2 + z_-^2) \vec{\Phi}_T^2 + m_\ell^2 \Phi_0^2}_T \\ &\quad + \underbrace{\left[ \vec{\Phi}_T \times \frac{\vec{q}_{T1}}{|\vec{q}_T|} \right]^2 - \left( \frac{\vec{\Phi}_T \cdot \vec{q}_{T1}}{|\vec{q}_{T1}|} \right)^2}_{TT'} \\ &\quad \left. + \underbrace{4z_+ z_- (z_+ - z_-) \Phi_0 (\vec{q}_{T1} \vec{\Phi}_T)}_{LT} \right]. \end{aligned} \quad (2.25)$$

Here we indicated the terms corresponding to photon 1 being in the longitudinal or transverse polarization states and the respective interference contributions.

Some comments on the applicability of the proposed formalism are in order.

Firstly, limitations due to energy-momentum conservation can be important in some regions of the phase space. We impose explicitly the kinematical limitations on the masses of the produced dissociative systems

$$\begin{aligned} W_{\gamma_1 p_2} &= \sqrt{s_{\gamma_1 p_2}} = \sqrt{x_1 s - \vec{q}_{T1}^2} > M_Y + M_{\ell\ell} > M_Y, \\ W_{\gamma_2 p_1} &= \sqrt{s_{\gamma_2 p_1}} = \sqrt{x_2 s - \vec{q}_{T2}^2} > M_X + M_{\ell\ell} > M_X \end{aligned} \quad (2.26)$$

for elastic-inelastic (first), inelastic-elastic (second) or inelastic-inelastic (both) contributions. Here the invariant mass of the dilepton system is given by

$$M_{\ell\ell}^2 = m_{\perp+}^2 + m_{\perp-}^2 + 2m_{\perp+} m_{\perp-} \cosh(y_+ - y_-) - (\vec{p}_{T+} + \vec{p}_{T-})^2. \quad (2.27)$$

In practice the phase-space constraint of Eq. 2.26 is very weak, as the distributions of interest are falling sufficiently fast.

---

<sup>2</sup>We correct a typo in the longitudinal photon contribution in [9].

Secondly, the evaluation of off-shell matrix elements explicitly uses the smallness of Sudakov parameters given in Eq. 2.17 in the expansion of the photon momenta. In order to be able to approximate e.g.  $q_1 = x_1 p_1 + q_{1\perp}$ , one should make sure that the condition

$$x_1 \gg \frac{M_X^2 - m_A^2 + \vec{q}_{T1}^2 + x_1 m_A^2}{(1 - x_1)s} \quad (2.28)$$

is fulfilled (a similar constraint with  $1 \leftrightarrow 2, M_X \leftrightarrow M_Y$  must hold for  $x_2$ ). This constraint in practice means that at a given center-of-mass energy, one should not go to too large invariant masses of the proton remnant. For photons coupling to an elastic transition the form factor cutoff on  $\vec{q}_{T1}^2$  is strong enough to ensure that Eq. 2.28 is very well fulfilled in the energy regime of interest.

## 2.4 Decorrelation of leptons

The  $k_T$ -factorization formulation is especially well suited to the description of pair production in the region of phase space where the total transverse momentum  $\vec{p}_{T\text{sum}} = \vec{p}_{T+} + \vec{p}_{T-}$  of the lepton pair is non vanishing. In the case of intact protons in the final state, the back-to-back correlation of leptons is very strong and in fact an equivalent photon approximation with collinear photons would have been of sufficient accuracy.

The situation is different however in the processes with inelastic excitation of the proton, where a large transverse momentum can be transferred via the photon exchange.

Let us look at the situation when one of the protons stays intact, while the other one dissociates. We can then obtain a very simple form for the cross section in the limit that the decorrelation momentum  $\vec{p}_{T\text{sum}}$  is much larger than the cutoff in the elastic form factor  $\Lambda \sim 0.7$  GeV. In this limit, we can neglect inside the matrix element  $B$  the transverse momentum of the photon coupling to the “elastic” proton and hence integrate out one of the photon transverse momenta. The decorrelation momentum  $\vec{p}_{T\text{sum}}$  is then exactly equal to the transverse momentum carried by the second photon. Neglecting lepton masses (which is anyway appropriate in the kinematic region of interest in this paper), we obtain the compact form for the cross section

$$\frac{d\sigma(AB \rightarrow A\ell^+\ell^-X)}{dy_+ dy_- d^2\vec{p}_{T+} d^2\vec{p}_{T-}} = n(x_1) \frac{\alpha_{\text{em}}^2 \mathcal{F}^{(\text{inel})}(x_2, \vec{p}_{T+} + \vec{p}_{T-})}{(\vec{p}_{T+} + \vec{p}_{T-})^2} \frac{2z_+ z_- (z_+^2 + z_-^2)}{\vec{p}_{T+}^2 \vec{p}_{T-}^2}. \quad (2.29)$$

Here

$$n(x_1) = \int \frac{d^2\vec{q}_{T1}}{\pi \vec{q}_{T1}^2} \mathcal{F}^{(\text{el})}(x_1, \vec{q}_{T1}) \quad (2.30)$$

is the Weizsäcker-Williams flux of photons in the elastically scattered proton. This result is fully analogous to the decorrelation momentum distribution of  $q\bar{q}$  dijets in the photon-gluon fusion obtained in [12].

## 3 Results of $k_T$ -factorization approach

In this section we present results obtained within the  $k_T$ -factorization approach discussed in the previous section. We have written a new code called PPTOLL based on the  $k_T$ -factorization formalism which performs all the integrations with the help of VEGAS method



Contribution	Low $p_T$ ( $p_T > 3$ GeV)		High $p_T$ ( $p_T > 15$ GeV)	
	SU	FFJLM	SU	FFJLM
elastic-elastic	16.39	–	0.297	–
elastic-inelastic	10.82	10.28	0.300	0.302
inelastic-elastic	10.82	10.28	0.300	0.302
inelastic-inelastic	9.25	6.39	0.329	0.301

**Table 1.** Cross section (in pb) for  $\mu^+\mu^-$  production for two different sets of  $p_T$  cuts and two different structure function models at  $\sqrt{s} = 7$  TeV. The additional cuts of  $|\eta(\mu^\pm)| < 2.5$ , and  $M_X = [1.07, 1000.00]$  GeV are used in all cases.

[13] and calculates many differential distributions, both of single-particle type as well as of correlation type. The code used by us is similar to the one developed for production of  $c\bar{c}$  quarks (e.g., see Ref. [14]).

Let us start the presentation of our results for integrated cross sections. In Table 1 we present integrated cross sections for two different sets of cuts for single muons:

They will be called *low  $p_T$*  ( $p_T > 3$  GeV) and *high  $p_T$*  ( $p_T > 15$  GeV) in the following for brevity. We have collected results with different deep-inelastic structure functions [3–5]. While for the low- $p_T$  cuts the elastic-elastic contribution dominates, for the high- $p_T$  cuts all contributions are of the similar size. The Szczurek-Uleshchenko (SU)  $F_2$  structure function [3] gives larger cross section than, e.g., the parametrization obtained by Fiore et al. [5] of the CLAS collaboration data. The numbers presented in Table 1 obtained with the code PPTOLL agrees with the Monte Carlo code LPAIR [7]. We note large differences between results obtained with the SU and the parametrizations by Fiore et al (labeled as FFJLM) [5] for inelastic-inelastic contribution for different models of  $F_2$  structure functions, especially for high- $p_T$  cuts. We shall return to this point in the conclusion section.

In Figure 2 we present distributions in transverse momentum of muons. The distributions drop quickly with growing muon transverse momentum. Different contributions have fairly similar shapes. This reflects matrix element dependence on muon transverse momentum which is the same for different components.

Figure 3 presents the corresponding distributions in muon rapidity. While elastic-elastic and inelastic-inelastic contributions are symmetric with respect to  $y = 0$ , the mixed contributions have maxima at  $y > 0$  (elastic-inelastic) or  $y < 0$  (inelastic-elastic).

Now we go to correlation observables which are particularly interesting and can be studied conveniently in our formalism. The invariant mass distribution shown in Figure 4 is a first example. All different contributions have similar shapes.

In Figure 5 we show distribution in transverse momentum of the muon pair. The elastic-elastic contribution is peaked sharply at  $p_{T\text{sum}} \approx 0$ , while other contributions have long tails towards large  $p_{T\text{sum}}$ . In the collinear approximation used, e.g., in Ref. [15], the transverse momenta of two muons are fully balanced and this type of distributions cannot be studied in that approximation.

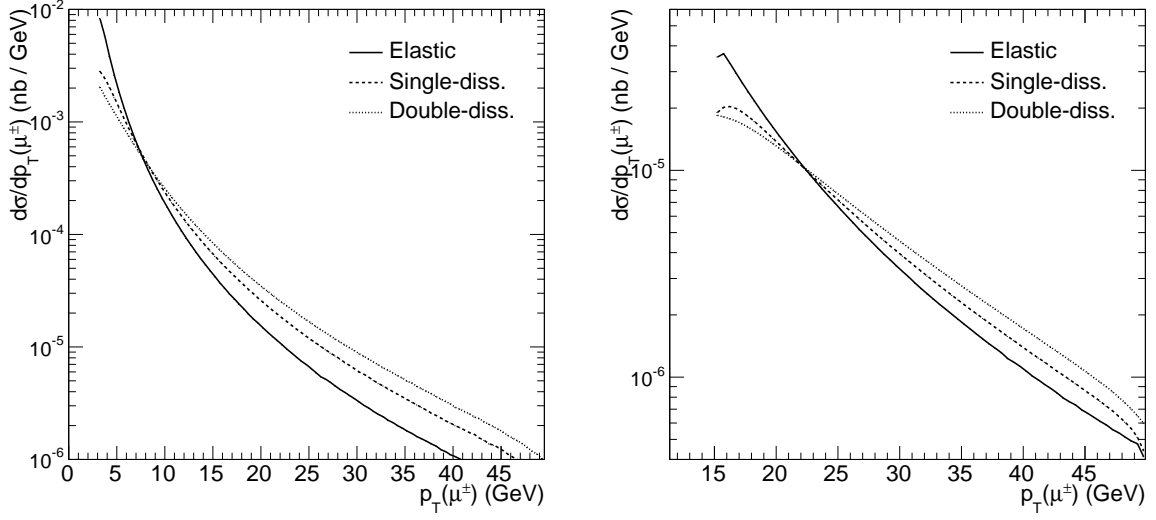


**Figure 2.** Muon transverse momentum distributions for low- $p_T$  (left) and high- $p_T$  (right) cuts. The different lines represent elastic-elastic (solid), elastic-inelastic (dashed), inelastic-elastic (dotted) and inelastic-inelastic (dash-dotted) mechanism at  $\sqrt{s} = 7$  TeV. The additional cuts of  $p_T(\mu^\pm) < 50$  GeV,  $|\eta(\mu^\pm)| < 2.5$ , and  $M_X = [1.07, 1000.00]$  GeV are used in all cases.

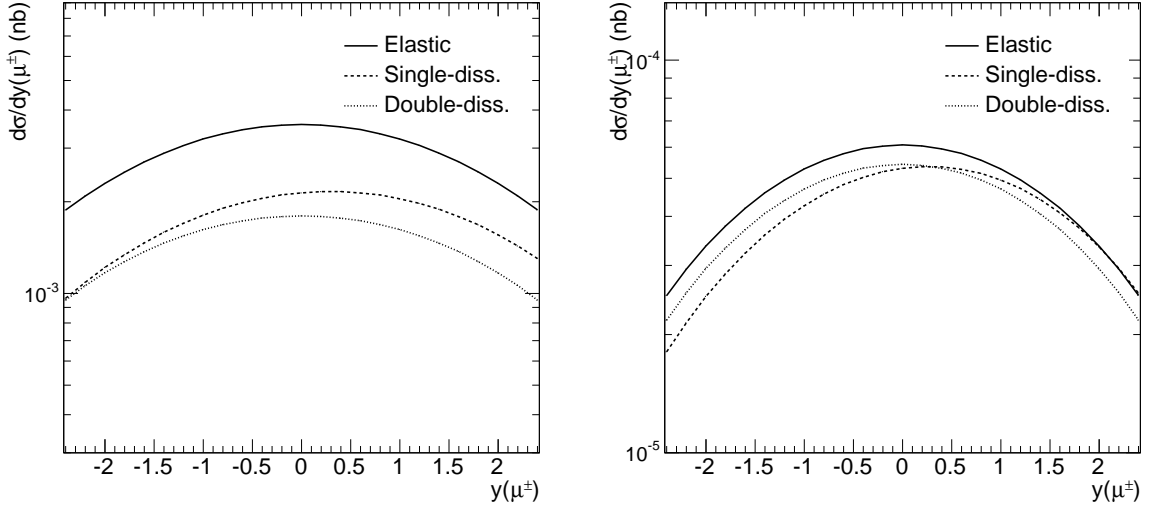


**Figure 3.** Muon rapidity distributions for low- $p_T$  (left) and high- $p_T$  (right) cuts at  $\sqrt{s} = 7$  TeV. The meaning of the curves is the same as in Figure 2. The additional cuts of  $p_T(\mu^\pm) < 50$  GeV,  $|\eta(\mu^\pm)| < 2.5$ , and  $M_X = [1.07, 1000.00]$  GeV are used in all cases.

Finally, Figure 6 shows the azimuthal correlations between outgoing  $\mu^+$  and  $\mu^-$ . The elastic-elastic contribution is sharply peaked at  $\Delta\phi \approx \pi$  while two other distributions have long tails down to  $\Delta\phi = 0$ .

Different models of structure functions have been proposed in the literature for  $F_2$

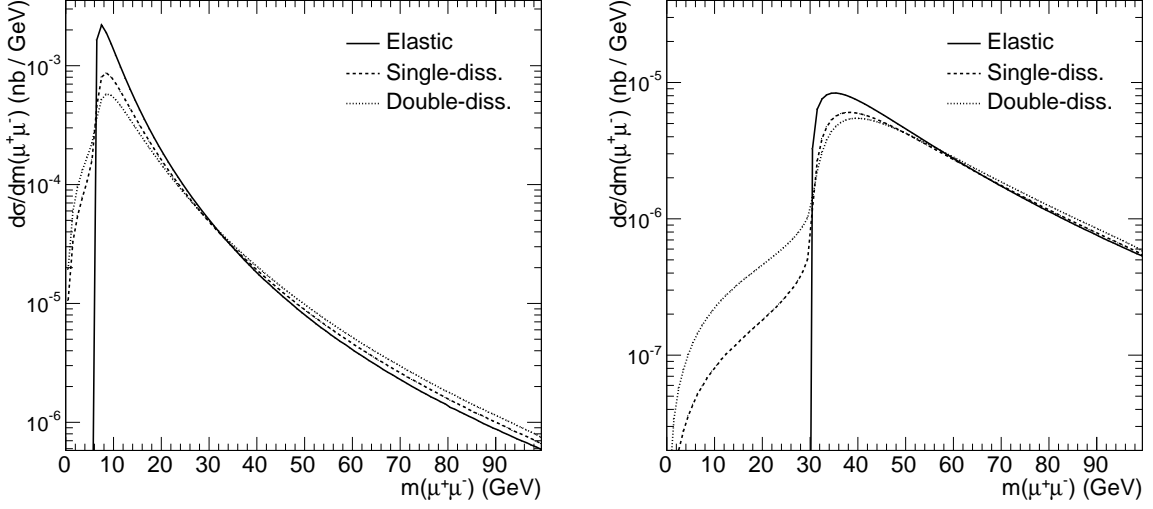


**Figure 4.** Muon pair invariant mass distributions for low- $p_T$  (left) and high- $p_T$  (right) cuts at  $\sqrt{s} = 7$  TeV. The meaning of the curves is the same as in Figure 2. The additional cuts of  $p_T(\mu^\pm) < 50$  GeV,  $|\eta(\mu^\pm)| < 2.5$ , and  $M_X = [1.07, 1000.00]$  GeV are used in all cases.

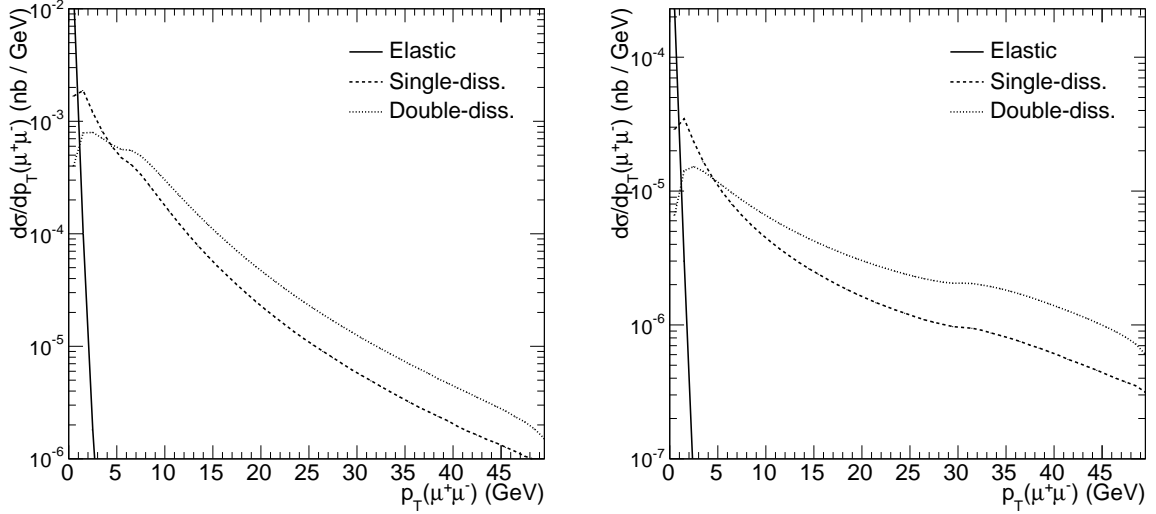


**Figure 5.** Muon pair transverse momentum distributions for low- $p_T$  (left) and high- $p_T$  (right) cuts at  $\sqrt{s} = 7$  TeV. The meaning of the curves is the same as in Figure 2. The additional cuts of  $p_T(\mu^\pm) < 50$  GeV,  $|\eta(\mu^\pm)| < 2.5$ , and  $M_X = [1.07, 1000.00]$  GeV are used in all cases.

structure function in broad range of  $x$  and  $Q^2$ . In different phase space regions, defined mostly by experimental cuts, one tests  $F_2$  in different ranges of its arguments.

Let us concentrate now on the region of large transverse momentum of the pair. In this region, as discussed above, the elastic-elastic contribution gives negligible contribution and inelastic contributions have to be considered.

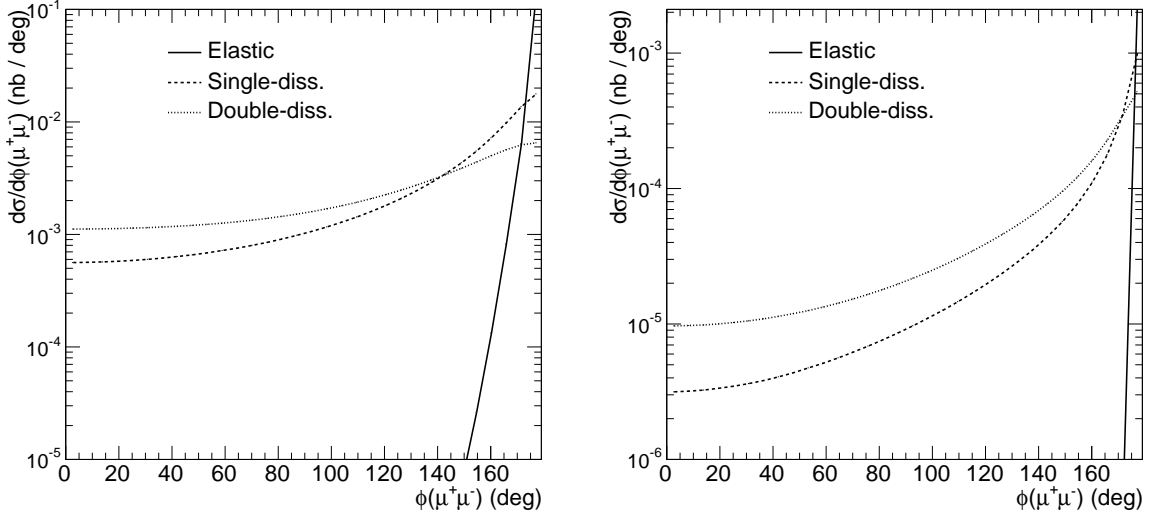


**Figure 6.** Distribution in azimuthal angle between muons for low- $p_T$  (left) and high- $p_T$  (right) cuts at  $\sqrt{s} = 7$  TeV. The meaning of the curves is the same as in Figure 2. The additional cuts of  $p_T(\mu^\pm) < 50$  GeV,  $|\eta(\mu^\pm)| < 2.5$ , and  $M_X = [1.07, 1000.00]$  GeV are used in all cases.

We first consider the mixed components (elastic-inelastic or inelastic-elastic). In Figure 7 we show two-dimensional distributions in transverse momentum of the muon pair ( $p_{T\text{sum}}$ ) and transverse momentum of one of the virtual photons. We observe a strong correlation between  $p_{T\text{sum}}$  and transverse momentum of the “inelastic photon” (the photon which leaves proton in the excited state). For this photon the virtuality is  $Q_i^2 \approx -q_{i,t}^2$ . Large transverse momentum means therefore also large virtuality. For large virtualities partonic structure functions which undergo QCD DGLAP evolution are adequate. The SU structure function, which in this region is just partonic  $F_2$ , is therefore a better choice than the Suri-Yennie (SY) parametrization [16] used in the LPAIR event generator [7], which is adequate for small  $Q^2$  and does not guarantee correct dependence at large  $Q^2$ . Then, standard well-known partonic structure functions should be rather used.

For inelastic-inelastic component the situation is, however, more complicated as is shown in Figure 8. One can observe two characteristic ridges around the diagonal  $p_{T\text{sum}} = q_{it}$  and for small  $q_{1T} \approx 0$  or  $q_{2T} \approx 0$ .

To understand the two-ridge structures of Fig. 8, in Fig. 9 we show a two-dimensional map in  $(q_{1T}, q_{2T})$ . The corresponding cross section is peaked along  $q_{1T}$  and  $q_{2T}$  axes, where in tails  $q_{1T}$  is small and  $q_{2T}$  is large or  $q_{1T}$  is large and  $q_{2T}$  is small. One clearly sees that for inelastic-inelastic contribution, even at large  $p_{T\text{sum}}$ , unlike for mixed components one is sensitive to low virtuality physics of resonance production. Therefore, a careful treatment of the low-virtuality region of  $F_2$  is for inelastic-inelastic component particularly important. Further studies are clearly needed.

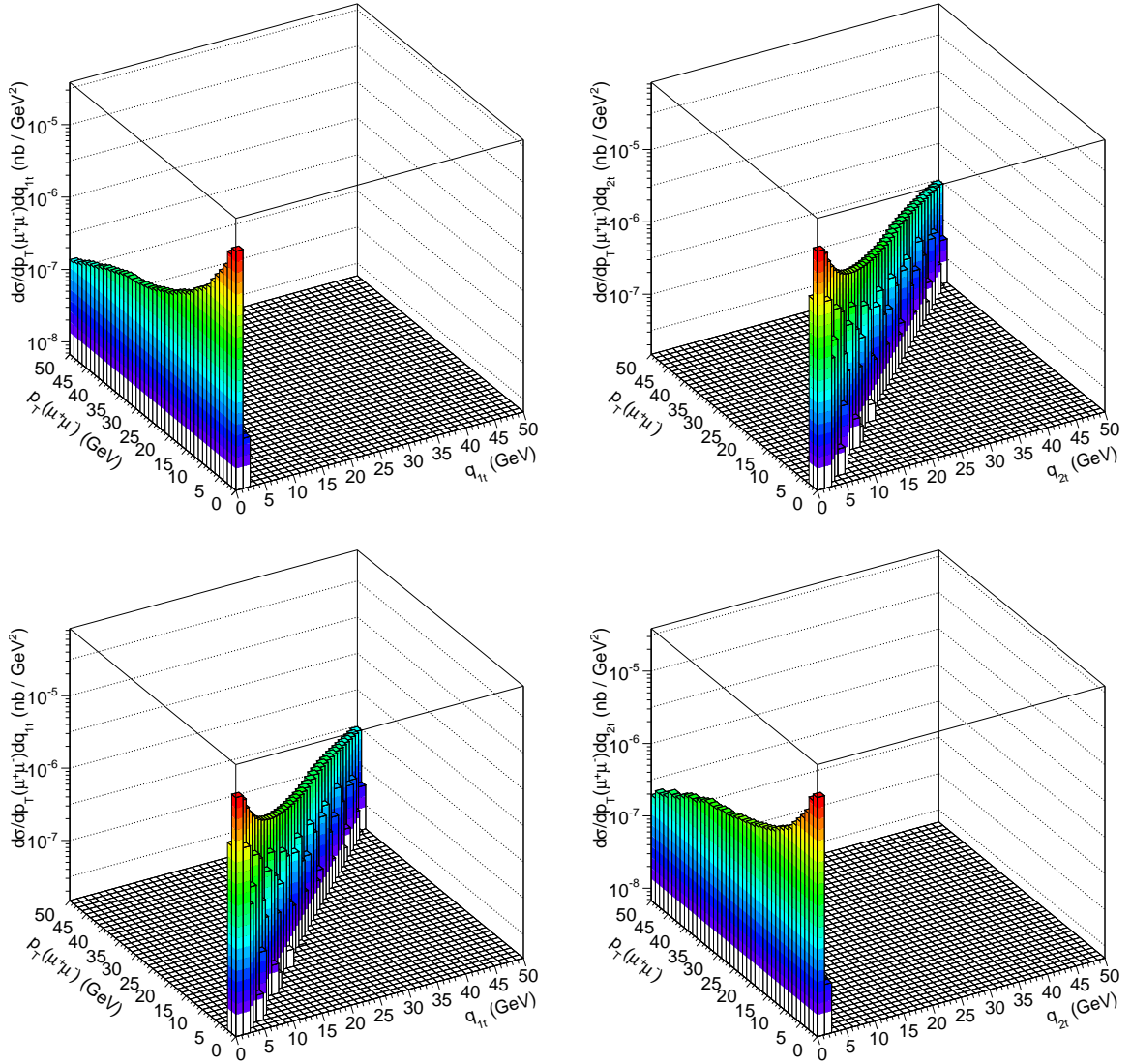


**Figure 7.** Two-dimensional distribution in  $p_{T\text{sum}}$  and one of transverse momentum ( $q_{1T}$  or  $q_{2T}$ ) of the virtual photon for elastic-inelastic (top row) and inelastic-elastic (bottom row) components at  $\sqrt{s} = 7$  TeV. The additional cuts of  $p_T(\mu^\pm) < 50$  GeV,  $|\eta(\mu^\pm)| < 2.5$ , and  $M_X = [1.07, 1000.00]$  GeV are used.

## 4 LPAIR Monte Carlo studies

### 4.1 LPAIR event generator

We performed an additional study using the LPAIR Monte Carlo (MC) event generator, which accounts for the electromagnetic production of lepton pairs in  $e^+e^-$ ,  $ep$  and  $pp$ <sup>3</sup> collisions [7, 8]. One should note that the LPAIR generator does not take into account

<sup>3</sup>In fact, the second colliding proton is treated in LPAIR only elastically, since there is no calculation for the dissociation of both protons in original version of the code.

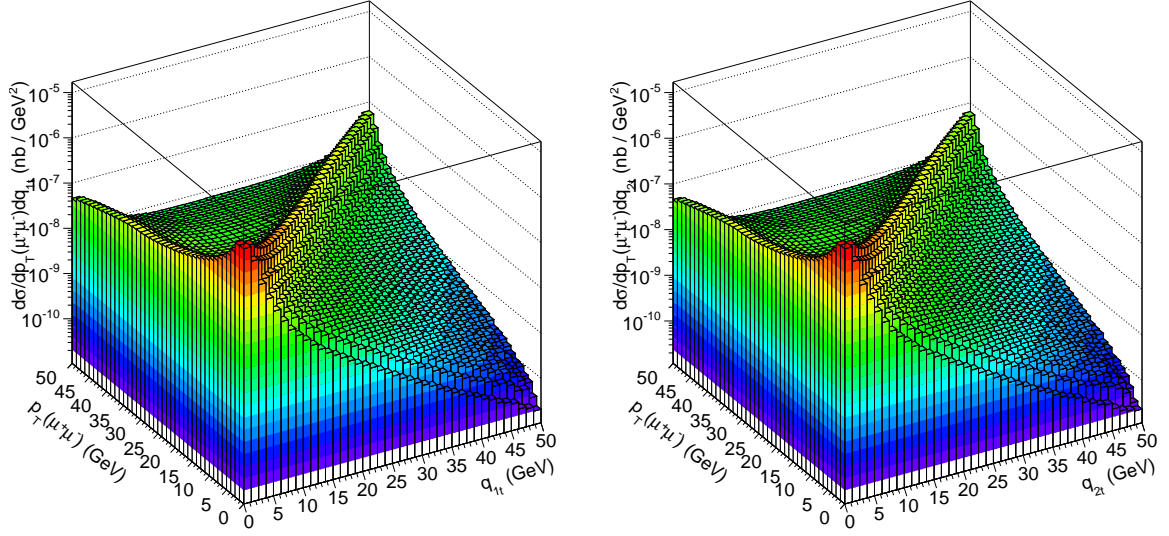


**Figure 8.** Two-dimensional distribution in  $p_{T\text{sum}}$  and one of transverse momentum of the virtual photon for inelastic-inelastic component at  $\sqrt{s} = 7$  TeV for  $p_{1T}, p_{2T} > 15$  GeV. The additional cuts of  $p_T(\mu^\pm) < 50$  GeV,  $|\eta(\mu^\pm)| < 2.5$ , and  $M_X = [1.07, 1000.00]$  GeV are used.

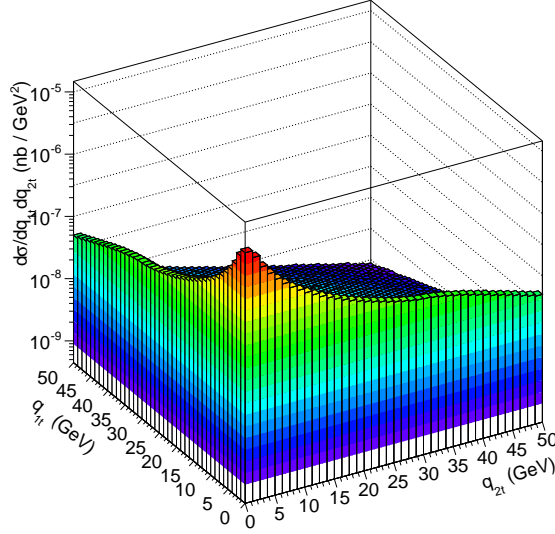


**Figure 9.** Two-dimensional distribution in  $(q_{1T}, q_{2T})$  for inelastic-inelastic component at  $\sqrt{s} = 7$  TeV and for  $p_{1T}, p_{2T} > 15$  GeV. The additional cuts of  $p_T(\mu^\pm) < 50$  GeV,  $|\eta(\mu^\pm)| < 2.5$ , and  $M_X = [1.07, 1000.00]$  GeV are used.

hadronic corrections to the cross sections, due to rescattering, for example. LPAIR has been extensively used by experiments at HERA, Tevatron and the LHC.

Instead of employing the equivalent photon approximation (EPA), LPAIR accounts for the two-photon interaction in a  $2 \rightarrow 4$  process by computing the full matrix element, e.g., for the  $pp \rightarrow p\ell^+\ell^-p$  diagram [8]. The hadronic structure of the proton is then

effectively taken into account by multiplying the proton charge by appropriate form factors or structure functions.

In the case of an exclusive production (Fig. 1a), the probability of a photon exchange from the proton is accounted by the electromagnetic form factor of the proton in the dipole approximation:

$$F_p(Q^2) = \frac{G_E(Q^2) + kG_M(Q^2)}{(1 + k)}, \quad (4.1)$$

where  $k = Q^2/4m_p^2$  and

$$G_E(Q^2) = \frac{1}{(1 + Q^2/0.71 \text{ GeV}^2)^2}, \quad (4.2)$$

$$G_M(Q^2) = \mu G_E(Q^2), \quad (4.3)$$

where  $G_E$  is the electric form factor and  $G_M$  the magnetic form factor of the proton, with  $\mu = 2.79$  being the proton magnetic moment.

On the other hand, in case of semi-exclusive production (Fig. 1b,c) the photon exchange leads to the proton break-up. Here, the SY parametrization is obtained from a fit to the available data for the total  $\gamma p$  cross section in the resonance region [16]. The data employed to obtain this parametrization corresponds to the measurements of the cross section of photonucleon processes and inelastic electron scattering, with center-of-mass energies up to  $\sqrt{s} \sim 20$  GeV. For the purpose of proton dissociation into a hadronic system, LPAIR is interfaced with the JETSET library of PYTHIA6 [18] in order to compute the kinematics of the final-state particles. Depending on the chosen structure function, the low-mass system can decay into  $\Delta^+$  and  $\Delta^{++}$  resonances while the high-mass system can decay into a larger multiplicity states with  $\Delta$ ,  $\eta$ , and  $K$  resonances.

The results obtained with LPAIR in general agree well with recent measurements of the two-photon production of dileptons in CMS [17]. One should note, however, that the predictions for the exclusive production are weakly dependent of the modeling the proton structure, and it is not the case for the semi-exclusive ones.

This paper will make use of large event samples produced for the exclusive and semi-exclusive two-photon production of dimuons in  $pp$  collisions at  $\sqrt{s} = 7$  TeV.

## 4.2 Some LPAIR results with detector acceptance

The study of the exclusive two-photon production of dimuons with the CMS detector has shown a good agreement of the LPAIR predictions with the data, but at the same time a significant disagreement was noticed for a part of the semi-exclusive production. As seen in Figure 6 of Ref. [19], the transverse momentum,  $p_{T\text{sum}}$ , distribution of the muon pairs in the high- $p_{T\text{sum}}$  region is not well described by LPAIR. Specifically, the LPAIR simulations do not reproduce the suppression seen in the data for dimuons with  $p_{T\text{sum}}$  above 10 GeV. This effect can potentially be connected to rescattering or absorption corrections which are not accounted for. In order to understand the possible source of the disagreement, we

Parametrization	$\sigma_{pp}(\gamma\gamma \rightarrow \mu^+\mu^-)$ (pb)	
	$p_T > 3$ GeV	$p_T > 15$ GeV
Elastic-Elastic	16.28	0.29
Inelastic-Elastic, Suri-Yennie	11.77	0.33
Inelastic-Elastic, Szczurek-Uleshchenko	9.87	0.30

**Table 2.** Production cross section obtained with the LPAIR code for the kinematic cuts of  $p_T(\mu^\pm) > 3$  or 15 GeV and the additional cuts of  $|\eta(\mu^\pm)| < 2.5$ , and  $M_X = [1.07, 1000.00]$  GeV in all cases.

perform here a more detailed study of the LPAIR predictions of semi-exclusive two-photon production of dimuons at  $\sqrt{s} = 7$  TeV.

As discussed in Sec. 4.1, the SY default parametrization of the proton structure function in LPAIR is based on data obtained with low incident energies, corresponding to the photon-proton center-of-mass energy  $\sqrt{s}$  between 1.11 and 18.03 GeV, and low photon virtualities – approximately  $Q^2 < 10$  GeV<sup>2</sup>. On the other hand, the data collected by the CMS Collaboration for the semi-exclusive two-photon production of dimuons evidently contain events involving very large photon virtualities. In particular, it concerns the region of the high  $p_{T\text{sum}}$  of the lepton pairs, where the disagreement is observed.

In order to test sensitivity of the LPAIR predictions to modeling of the structure function, we introduced a more recent parametrization available in the literature, such as the SU parametrization used already in the  $k_T$ -factorization approach. In the context of the experimental studies, we restrict the phase space by similar kinematic cuts as employed in Ref. [19]:  $p_T(\mu^\pm) > 3$  or 15 GeV and  $|\eta(\mu^\pm)| < 2.5$  for each muon and an invariant mass of the hadronic system,  $M_X$ , between 1.07 to 1000 GeV. As a result, event samples with one million events are produced at  $\sqrt{s} = 7$  TeV for each of the PDF parametrizations with the production cross sections presented in Tab. 2.

For the  $Q^2$  values below the range of validity of the parametrizations, the approach in the SU parametrization uses a shifted value ( $Q^2 + \mu^2$ ) of the factorization scale and is rescaled by a factor which ensures, that  $F_2 \rightarrow 0$  when  $Q^2 \rightarrow 0$ .

Figures 10 and 11 show the  $p_T$ , and pseudorapidity,  $\eta$ , distributions of single muons for the SY parametrization in comparison to the SU one with  $p_{T,min}$  of 3 and 15 GeV. One sees that the  $p_T$  distribution have an overall agreement, while the  $\eta$  distributions have significantly different shapes. This effect already shows that the integrated detector acceptance correction is sensitive to a choice of the parton densities.

Figure 12 and 13 show the distributions of the dimuon variables – the muon azimuthal angle difference and the pair transverse momentum. For high  $p_T(\mu^+\mu^-)$  the shapes are similar, whereas at the low  $p_T$  the differences are more pronounced. This region is related to the lower  $Q^2$  values, which depends on the approach used to describe the photons with low virtualities and explains the shift in the peaks for each parametrization around  $p_T \sim 1$  GeV. Similar effects are observed for the  $\Delta\phi$  distributions. For completeness, in Fig. 14 the distributions of the photon virtuality are compared.

To better clarify the origin of these differences, in the following the results obtained



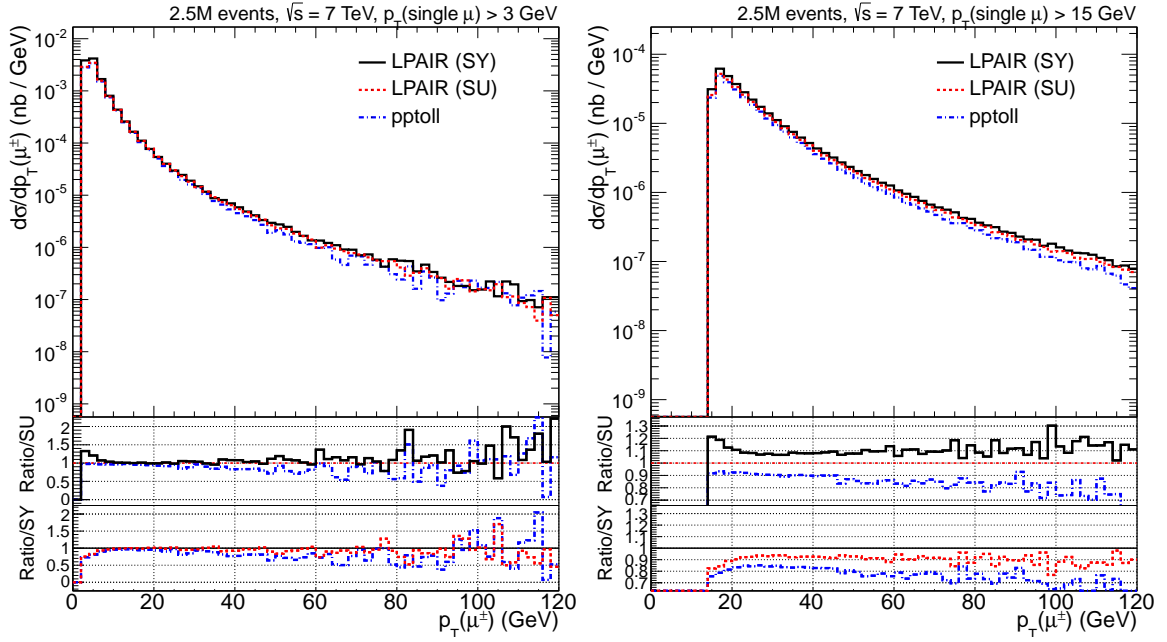


**Figure 10.** Transverse momentum distribution of muons in the final state taking into account a minimum cut of  $p_T(\mu^\pm) > 3$  (left) and  $p_T(\mu^\pm) > 15$  GeV (right) and also additional kinematic cuts of  $|\eta(\mu^\pm)| < 2.5$ , and  $M_X = [1.07, 1000.00]$  GeV in both cases. The distributions are obtained with LPAIR using SY (solid line) and SU (single-dashed line) structure functions, and with PPTOLL where the  $k_T$ -factorization approach was implemented (double-dashed line).

with LPAIR are compared to the complementary approach described in Section 3.

We are interested in better understanding the  $p_{T\text{sum}}$  spectra, which can be nicely studied within the  $k_T$ -factorization approach proposed in this paper, but cannot be addressed in simple EPA when transverse momenta of photons are neglected. Therefore, we wish to understand the correlation of the  $p_{T\text{sum}}$  with other kinematical variables. In Fig. 15 we show some examples of such two-dimensional correlations. In the upper plots, the distribution in  $M_X$  and  $p_{T\text{sum}}$  is shown for  $p_T > 3$  GeV (left) and for  $p_T > 15$  GeV (right). We observe that the shape in  $M_X$  strongly depends on  $p_{T\text{sum}}$ . At lower  $p_{T\text{sum}}$  the  $M_X$ -dependence is very sharp, while at higher  $p_{T\text{sum}}$  the dependence is much weaker.

The lower figures show distribution in  $(p_{T\text{sum}}, \Delta\phi)$ . One can observe clearly back-to-back type of correlations at small  $p_{T\text{sum}}$  and almost complete decorrelation for large  $p_{T\text{sum}}$  in the case of  $p_T > 3$  GeV (left). The case of  $p_T > 15$  GeV (right) is, however, much more complicated. One observes some areas which are forbidden due to kinematics.

## 5 LPAIR vs. $k_T$ -factorization approach

For a complete overview of the physics related to the two-photon production of dimuons, we compare results obtained with the new  $k_t$ -factorization approach (as described in Sec. 2) with the LPAIR code. In case of elastic-elastic events we observe good agreement within

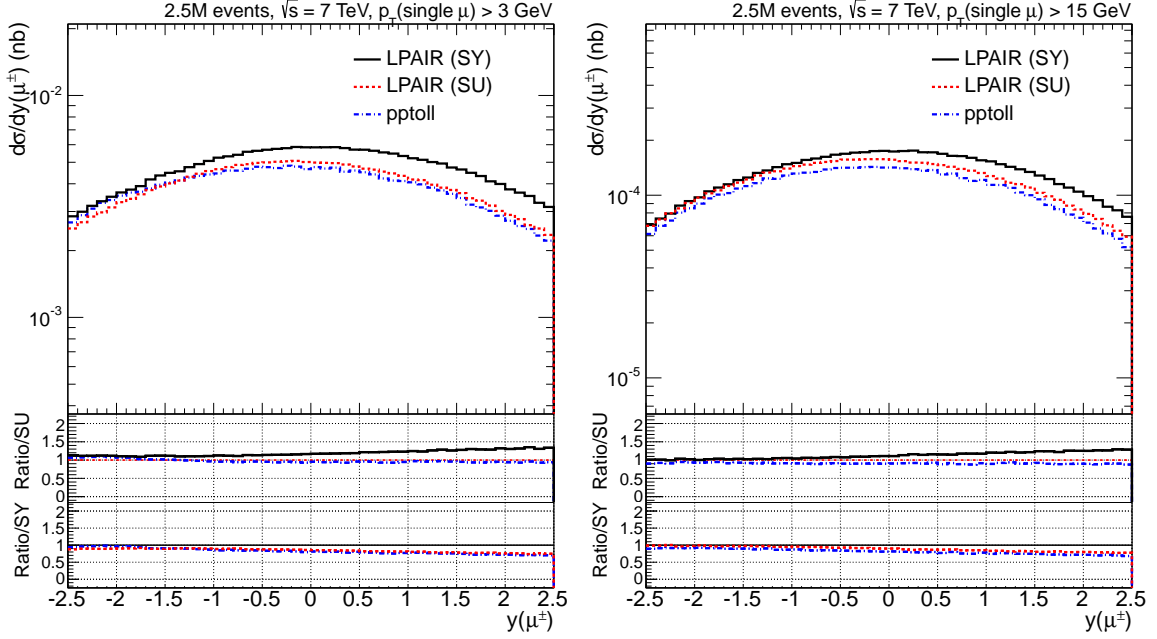


**Figure 11.** Rapidity distribution of dimuons in the final state taking into account  $p_T(\mu^\pm) > 3$  GeV (left) and  $p_T(\mu^\pm) > 15$  GeV (right) and also additional kinematic cuts of  $|\eta(\mu^\pm)| < 2.5$ , and  $M_X = [1.07, 1000.00]$  GeV in both cases. The distributions are obtained with LPAIR using SY (solid line) and SU (single-dashed line) structure functions, and with PPTOLL where the  $k_T$ -factorization approach was implemented (double-dashed line).

the kinematic cuts used in this study although the agreement gets somewhat worse when the  $p_T$ -cutoff gets larger.

In the following we concentrate on distributions for elastic-inelastic events, in which one proton dissociates while the other one stays intact. We now turn to a brief discussion of the differences between the  $k_T$ -factorization and LPAIR results. In the following, for the purpose of comparison, we shall in both approaches use only the  $F_2$  structure function. First of all, the  $F_1$  structure is not so well known at low scales and, secondly, it is only  $F_2$  which appears in the high-energy limit.

We begin with the comparison of the  $p_{T\text{sum}}$  distribution, shown in Figure 13, for both the low- $p_T$  and high- $p_T$  cuts. We observe some deviations in the shape of the distribution, especially for the high- $p_T$  cut, where there appears to be an overprediction of large- $p_{T\text{sum}}$  pairs, and a deficit at low  $p_{T\text{sum}}$  in the  $k_T$ -factorization approach with respect to the LPAIR results. This difference must be ascribed to the use of high-energy kinematics in the  $k_T$ -factorization approach.

Firstly, recall that due to experimental demands we integrate up to a very large mass of the excited system  $M_X = 1$  TeV. It is obvious that at such large  $M_X$ , the "small" Sudakov component of the "inelastic photon" [Eq. (2.17)] is no longer negligible with respect to the momentum fraction  $x$ . Among other things, this entails that momentum fractions  $x_{1,2}$  cannot be calculated from the muon kinematics alone, but must be calculated taking the

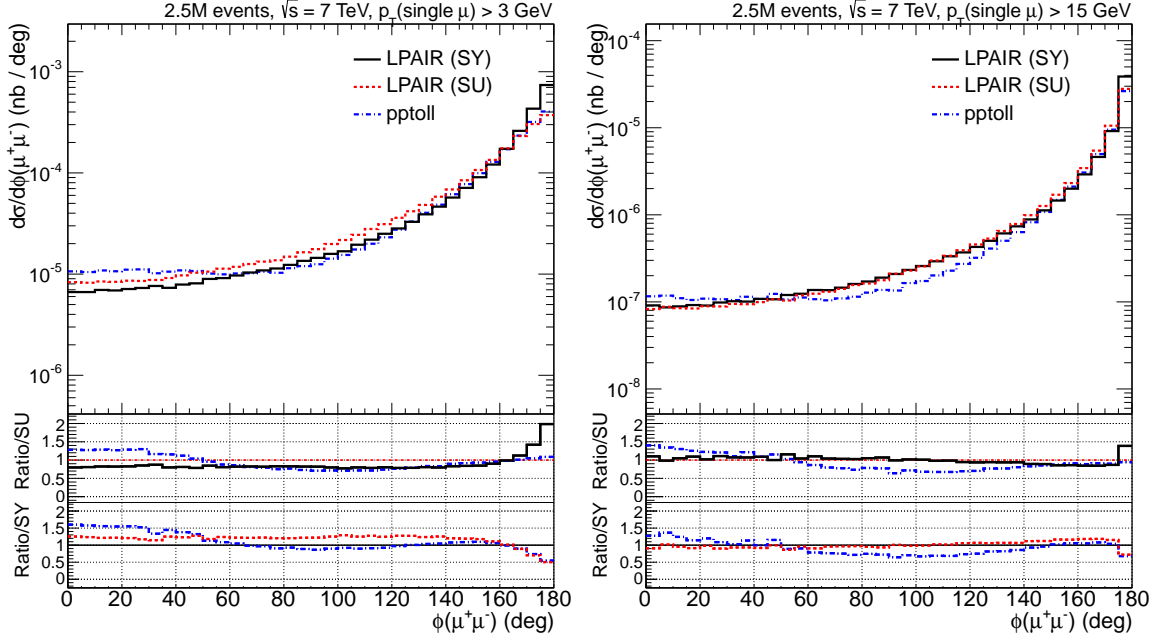


**Figure 12.**  $\Delta\phi(\mu^+\mu^-)$  distribution of muon pairs in the final state taking into account  $p_T(\mu^\pm) > 3$  GeV (left) and  $p_T(\mu^\pm) > 15$  GeV (right) and also additional kinematic cuts of  $|\eta(\mu^\pm)| < 2.5$ , and  $M_X = [1.07, 1000.00]$  GeV in both cases. The distributions are obtained with LPAIR using SY (solid line) and SU (single-dashed line) structure functions, and with PPTOLL where the  $k_T$ -factorization approach was implemented (double-dashed line).

full final state into account.

Secondly, in the most general case, the fluxes of longitudinal and transverse photons will differ [2], and a more involved decomposition in terms of the full density matrix of photons must be adopted.

Notice that these deviations are concentrated in a kinematical region of large longitudinal momentum transfers. In impact parameter space, this would correspond to a domain of intermediate to small impact parameters, where absorptive effects are expected to be important, and the theoretical uncertainty associated with them is arguably higher than the here observed deviations between the two approaches.

In the plots shown in Figs. 10–11 and 16, we present other kinematic distributions for both the  $k_T$ -factorization and LPAIR approaches. The similar comments as above apply as far as deviations between the two approaches are concerned.

## 6 Conclusions

In the present paper we have reviewed the production of muon pairs via the photon-photon fusion in proton-proton collisions at the LHC. All types of processes (elastic-elastic, elastic-inelastic, inelastic-elastic and inelastic-inelastic) have been discussed. We have performed the calculation with the code LPAIR supplemented by the proton structure functions. The

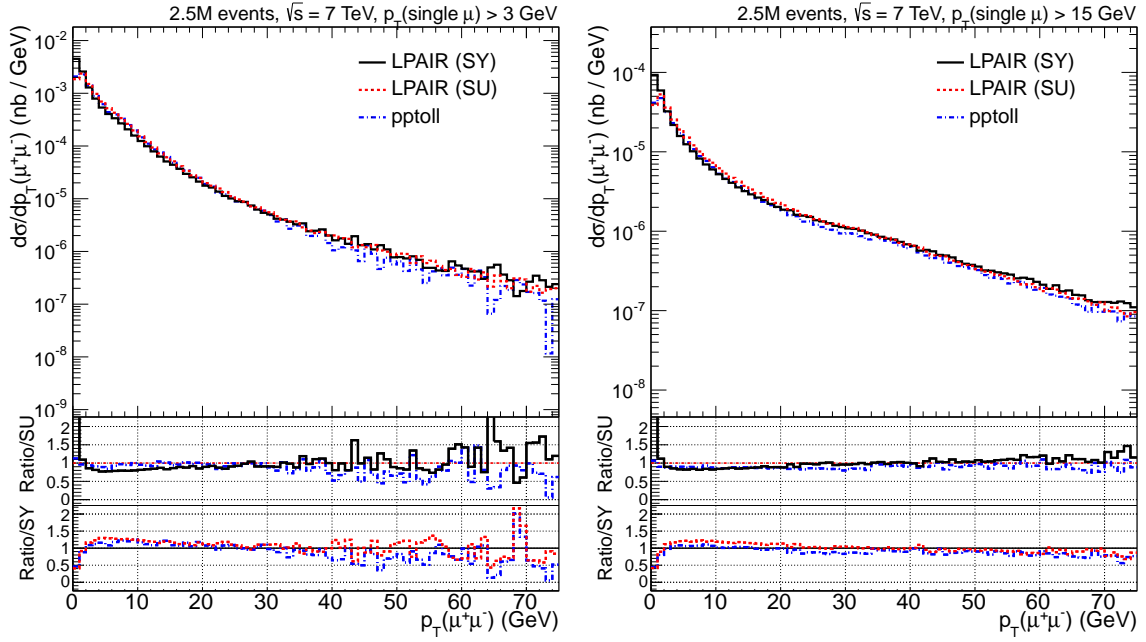


**Figure 13.** Transverse momentum distribution of dimuons taking into account  $p_T(\mu^\pm) > 3$  GeV (left) and  $p_T(\mu^\pm) > 15$  GeV (right) and also additional kinematic cuts of  $|\eta(\mu^\pm)| < 2.5$ , and  $M_X = [1.07, 1000.00]$  GeV in both cases. The distributions are obtained with LPAIR using SY (solid line) and SU (single-dashed line) structure functions, and with PPTOLL where the  $k_T$ -factorization approach was implemented (double-dashed line).

related uncertainties due to lack of precise knowledge of the latter objects have been studied and discussed.

We have also proposed a new, somewhat simplified, method to calculate the processes in terms of photon unintegrated distributions that depend on photon longitudinal fraction and its transverse momentum. The results of the calculation have been compared with the results obtained with the LPAIR code. Rather good agreement between the two approaches has been achieved. The formalism proposed by us can be used not only for calculating integrated cross section or single muon distribution, but is especially well suited for efficient calculation of correlation observables. As a results, the  $k_T$ -factorization approach can be extend to allow the study of the absorption corrections in inelastic collisions.

We have calculated distributions in dimuon invariant mass, in transverse momentum of the muon pair and in relative azimuthal angle between outgoing muons. The calculation has been performed separately for different components and different proton structure functions from the literature. If the cuts on muon transverse momenta are imposed all components (elastic-elastic, elastic-inelastic, inelastic-elastic, inelastic-inelastic) give similar contribution. While the elastic-elastic contribution is well under control, the inelastic contributions are subjected to uncertainties of the order of 20% or even more for some regions of correlation observables. We have now at our disposal a good tool to calculate dileptons as a background to many other Standard Model processes. In many cases such

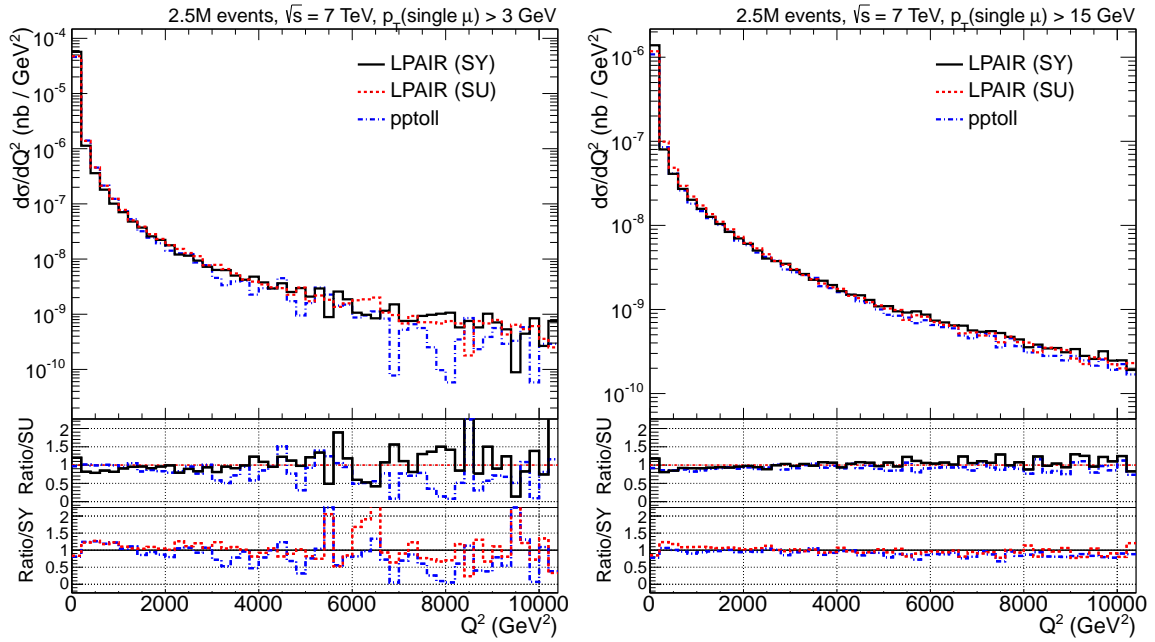


**Figure 14.** Photon virtuality distribution taking into account the cuts  $p_T(\mu^\pm) > 3$  GeV (left) and  $p_T(\mu^\pm) > 15$  GeV (right) and also additional kinematic cuts  $|\eta(\mu^\pm)| < 2.5$ , and  $M_X = [1.07, 1000.00]$  GeV in both cases. The distributions are obtained with LPAIR using SY (solid line) and SU (single-dashed line) structure functions, and with PPTOLL where the  $k_T$ -factorization approach was implemented (double-dashed line).

a background was not even estimated. Similar method could be used for other photon-initiated processes.

We have shown that different regions of phase space are sensitive to structure functions in different ranges of  $x$  (longitudinal momentum fraction) and  $Q^2$  (scale). At present, there is no one set of structure functions in the literature which correctly treats all regions of  $x$  and  $Q^2$ . We have used different sets of proton structure functions from the literature and quantified uncertainties for cross section predictions for  $\mu^+\mu^-$  production. They are typically of the order of 20%–30%, and, although a significant sensitivity to the parton distribution function is observed, it cannot explain high- $p_T$  results obtained by the CMS Collaboration.

In case of the semi-exclusive events at large  $p_T$  of the pair absorption effects must be included in the calculation. We do not need to mention that the calculation of such effects in terms of kinematic variables is not an easy task. While some early discussions of absorptive effects in lepton pair production do exist [20, 21], these studies concentrate on an entirely different kinematic region than in this work. It therefore needs to be understood whatever such absorption effects could be *extracted* by comparison of the calculated cross sections with the measured ones. This subject will be studied in more detail in the future.

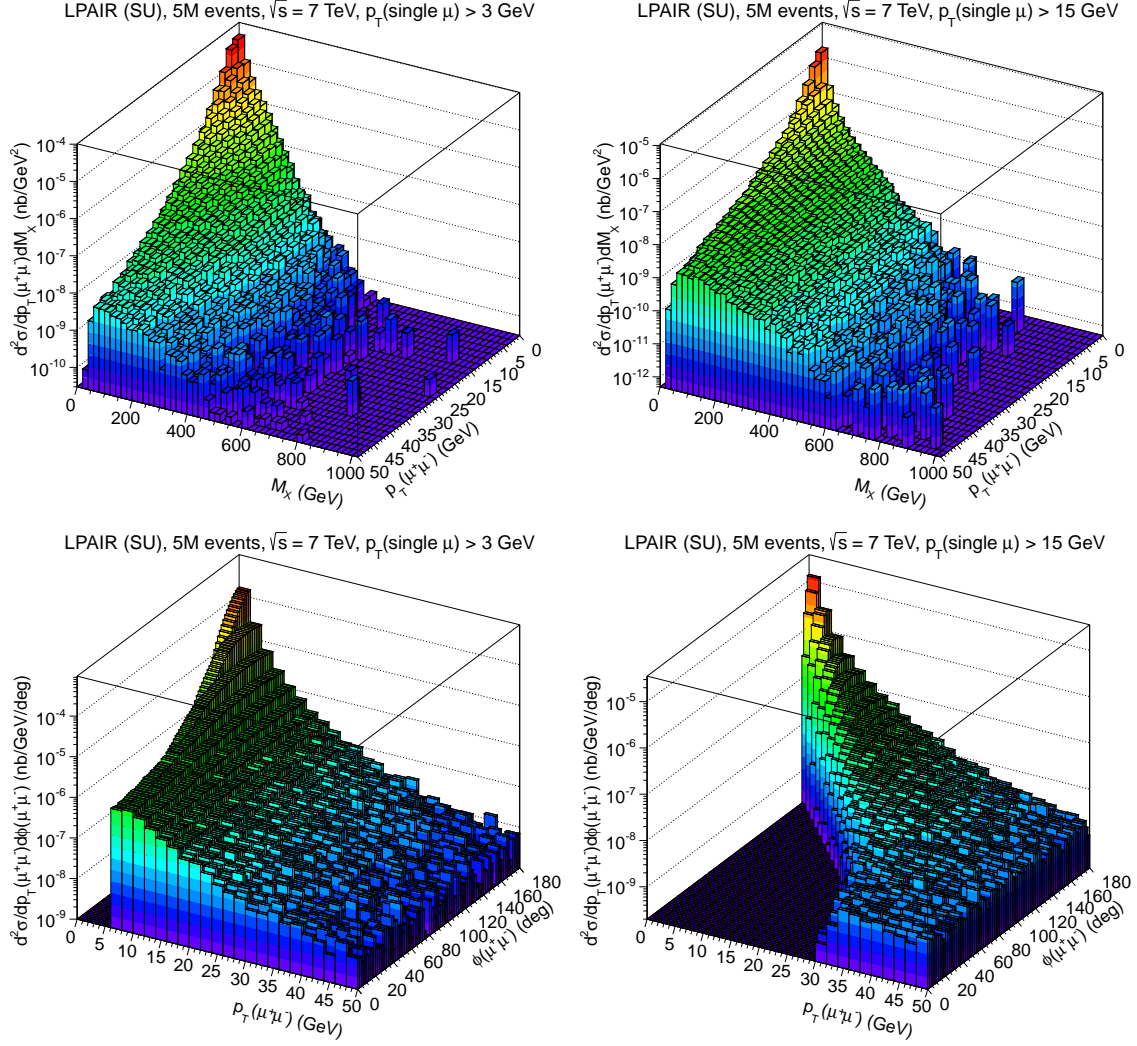


**Figure 15.** Different two-dimensional correlation of  $p_{T\text{sum}}$  with  $M_X$  (upper plots) and with  $\Delta\phi$  (lower plots) for  $p_T > 3$  GeV (left side) and for  $p_T > 15$  GeV (right side) obtained with SU parametrization. In addition, we apply in both cases kinematical cuts of  $|\eta(\mu^\pm)| < 2.5$ , and  $M_X = [1.07, 1000.00]$  GeV.

## Acknowledgments

We are indebted to Rafał Maciuła for help in preparing a Monte Carlo version of the code calculating lepton production in the  $k_T$ -factorization approach. The authors strongly acknowledge the support by the dedicated bilateral project between the FNRS in Belgium and PAN in Poland. GGS thanks the partial support by CNPq and Capes, Brazil. This work was partially supported by the Polish MNiSW grant DEC-2011/01/B/ST2/04535 as well as by the Centre for Innovation and Transfer of Natural Sciences and Engineering Knowledge in Rzeszów.

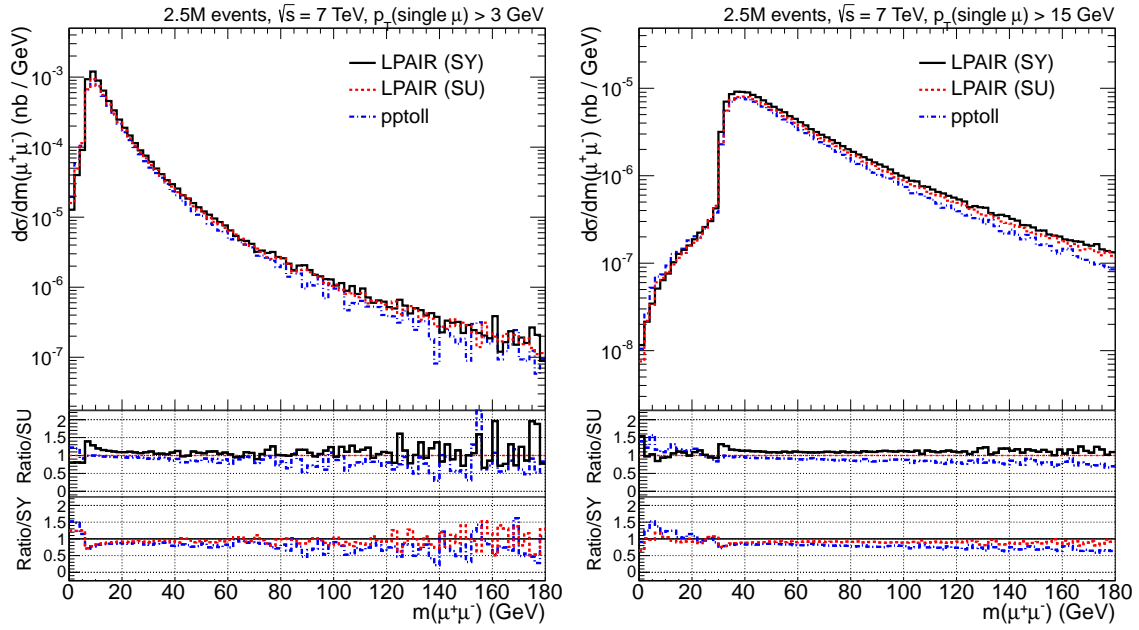


**Figure 16.** Invariant mass distributions for muon pairs obtained with LPAIR (solid and single-dashed line) in comparison to the  $k_T$ -factorization predictions (double-dashed line) for the interaction of off-shell photons as described in Sec. 2 taking into account kinematics cuts of  $p_T > 3$  GeV (left column) and  $p_T > 15$  GeV (right column) for inelastic collisions. The histograms are the results obtained with LPAIR using SY (solid line) and SU (single-dashed line) structure functions, and with PPTOLL implementing the  $k_T$  factorization algorithm (double-dashed line). All distributions are obtained with the kinematic cuts of  $|\eta(\mu^\pm)| < 2.5$ , and  $M_X = [1.07, 1000.00]$  GeV.

## References

- [1] V. M. Budnev, I. F. Ginzburg, G. V. Meledin and V. G. Serbo, *The process  $pp \rightarrow ppe^+e^-$  and the possibility of its calculation by means of quantum electrodynamics only*, *Nucl. Phys.* **B63** (1973) 519.
- [2] V.M. Budnev, I.F. Ginzburg, G.V. Meledin, V.G. Serbo, *The Two photon particle production mechanism. Physical problems. Applications. Equivalent photon approximation*, *Phys. Rept.* **15** (1975) 181.
- [3] A. Szczurek and V. Uleshchenko, *Nonpartonic components in the nucleon structure functions at small  $Q^2$  in the broad range of  $x$* , *Eur. Phys. J.* **C12** (2000) 663, arxiv:hep-ph/9904288.
- [4] A. Szczurek and V. Uleshchenko, *On the range of validity of the QCD improved parton model*, *Phys. Lett.* **B475** (2000) 120, arxiv:hep-ph/9911467.
- [5] R. Fiore, A. Flachi, L. L. Jenkovszky, A. I. Lengyel and V. K. Magas, *Explicit model realizing parton hadron duality*, *Eur. Phys. J.* **A15**, 505 (2002), arxiv:hep-ph/0206027.
- [6] R. Maciula and A. Szczurek, *Open charm production at the LHC -  $k_t$ -factorization approach* *Phys. Rev.* **D87** (2013) 094022, arxiv:1301.3033 [hep-ph].
- [7] S.P. Baranov, O., Dünger, H., Shooshtari, J.A.M. Vermaseren; LPAIR: *A generator for lepton pair production*, *Proceedings of Physics at HERA* **3** 1478.



- [8] J.A.M. Vermaseren, *Two Photon Processes at Very High-Energies*, *Nucl. Phys.* **B229** (1983) 347.
- [9] E. Bartos, S. R. Gevorkyan, E. A. Kuraev and N. N. Nikolaev, *The lepton pair production in heavy ion collisions in perturbation theory*, *Phys. Rev.* **A66**, 042720 (2002), arxiv:hep-ph/0109281.
- [10] G. V. Frolov, V. N. Gribov and L. N. Lipatov, *Phys. Lett. B* **31**, 34 (1970) ;  
L. N. Lipatov and G. V. Frolov, *Pisma Zh. Eksp. Teor. Fiz.* **10**, 399 (1969).
- [11] H. Cheng and T. T. Wu, *Phys. Rev. D* **1**, 456 (1970).
- [12] A. Szczurek, N. N. Nikolaev, W. Schäfer and J. Speth, *Phys. Lett. B* **500**, 254 (2001) [hep-ph/0011281].
- [13] G.P. Lepage, *A New Algorithm for Adaptive Multidimensional Integration*, *J. Comp. Phys.* **27** (1978) 192.
- [14] M. Łuszczak and A. Szczurek, *Gluon transverse momenta and charm quark-antiquark pair production in  $p\bar{p}$  collisions at Tevatron*, *Phys. Rev.* **D73** (2006) 054028, arxiv:hep-ph/0512120.
- [15] R. Maciula, A. Szczurek and G. Ślipek, *Kinematical correlations of dielectrons from semileptonic decays of heavy mesons and Drell-Yan processes at BNL RHIC*, *Phys. Rev.* **D83** (2011) 054014, arxiv:1011.4207 [hep-ph].
- [16] A. Suri, D.R. Yennie, *The space-time phenomenology of photon absorption and inelastic electron scattering*, *Annals Phys.* **72** (1972) 243.
- [17] CMS Collaboration, *Exclusive photon-photon production of muon pairs in proton-proton collisions at  $\sqrt{s} = 7$  TeV*, *JHEP* **01** (2012) 052, arxiv:1111.5536 [hep-ex] ;  
CMS Collaboration, *Search for exclusive or semi-exclusive photon pair production and observation of exclusive and semi-exclusive electron pair production in pp collisions at  $\sqrt{s} = 7$  TeV*, *JHEP* **11** (2012) 080, arxiv:1209.1666 [hep-ex].
- [18] T. Sjöstrand, S. Mrenna, P. Z. Skands, *PYTHIA 6.4 Physics and Manual*, *JHEP* **05** (2006) 026.
- [19] CMS Collaboration, *Study of exclusive two-photon production of  $W^+W^-$  in pp collisions at  $\sqrt{s} = 7$  TeV and constraints on anomalous quartic gauge couplings*, *JHEP* **07** (2013) 116.
- [20] V.A. Khoze, A.D. Martin, R. Orava, M.G. Ryskin, *Luminosity monitors at the LHC*, *Eur. Phys. J.* **C19** (2001) 313, arxiv:hep-ph/0010163.
- [21] L.A. Harland-Lang, V.A. Khoze, M.G. Ryskin, W.J. Stirling, *The phenomenology of Central Exclusive Production at Hadron Colliders*, *Eur. Phys. J.* **C72** (2012) 2110, arXiv:1204.4803[hep-ph]